REPORT DOCUMENTATION PAGE

Form Approved
OMB NO. 0704-0188

1. AGENCY USE ONLY (Leave Blank)	2. REPORT DATE 8/01	3. REPORT TYPE AND DATES COVERED Final Technical Report 6/98-5/01

4. TITLE AND SUBTITLE
Investigation of III-Nitride Alloys for Ultraviolet Photodetectors and Blue-Green Lasers

5. FUNDING NUMBERS
N00014-98-1-0490

6. AUTHOR(S)

7. PERFORMING ORGANIZATION NAME(S) AND ADDRESS(ES)
Northwestern University
Center for Quantum Devices
2225 N. Campus Drive, Room 4051
Evasnton, IL 60208

8. PERFORMING ORGANIZATION REPORT NUMBER

9. SPONSORING / MONITORING AGENCY NAME(S) AND ADDRESS(ES)
Office of Naval Research
800 N. Quincy Street
Arlington, VA 22217-5660

10. SPONSORING / MONITORING AGENCY REPORT NUMBER

11. SUPPLEMENTARY NOTES
The views, opinions and/or findings contained in this report are those of the author(s) and should not be construed as an official Department of the Navy position, policy or decision, unless so designated by other documentation.

12 a. DISTRIBUTION / AVAILABILITY STATEMENT
Approved for public release; distribution unlimited.

12 b. DISTRIBUTION CODE

13. ABSTRACT (Maximum 200 words)

This AASERT contract was intended to support one graduate and one undergraduate students for three years, with the objective of conducting research work on the growth and characterization of wide bandgap GaN based semiconductors for ultraviolet photodetectors and visible light emitters. The research was directed toward optimizing the metalorganic chemical vapor deposition (MOCVD) growth and characterization of undoped, n-type and p-type doped wide bandgap GaN and $Al_xGa_{1-x}N$ semiconductors, for x ranging from 0 to 1, on sapphire substrates. The optical and electrical properties of GaN grown using two different organometallic precursors, TMGa and TEGa, have been compared. The fabrication and characterization of GaN and GaN:Mg MSM photodetectors, with high speed and visible rejection is reported. GaN p-i-n photodiodes with a UV-to-visible rejection ratio of 6 orders of magnitude were demonstrated. The responsivity of these devices was analytically modeled and allowed the extraction of the minority carrier diffusion length for electrons in the p-type GaN material. Highly efficient $Al_xGa_{1-x}N$ based visible blind and solar blind p-i-n photodiodes have been demonstrated which cover the widest spectral range ever reported, form 225 to 362 nm. By varying the doping of the GaInN active layer in GaInN/GaN double heterostructures, blue (525 nm) and green (560 nm) light emitting diodes were demonstrated and characterized.

14. SUBJECT TERMS			15. NUMBER OF PAGES
			16. PRICE CODE
17. SECURITY CLASSIFICATION OR REPORT **UNCLASSIFIED**	18. SECURITY CLASSIFICATION ON THIS PAGE **UNCLASSIFIED**	19. SECURITY CLASSIFICATION OF ABSTRACT **UNCLASSIFIED**	20. LIMITATION OF ABSTRACT **UL**

NSN 7540-01-280-5500

Standard Form 298 (Rev.2-89)
Prescribed by ANSI Std. 239-18
298-102

Table of Contents

I. INTRODUCTION

This AASERT contract was intended to support one graduate and one undergraduate students for three years, with the objective of conducting research work on the growth and characterization of wide bandgap GaN based semiconductors for ultraviolet photodetectors and visible light emitters.

The students contributed to research work directed toward optimizing the metalorganic chemical vapor deposition of GaN, AlGaN and InGaN semiconductors, developing the processing of the wafers into photodetectors and light emitting diodes, measuring the device performance and modeling the device operation. The outcome of the systematic work they conducted is summarized in this report.

II. GROWTH AND CHARACTERIZATION OF MATERIALS

II.1. $Al_xGa_{1-x}N$ based materials, structures and devices

III-Nitride semiconductors, such as AlN, GaN, InN and their alloys, have become the leading material system for wide bandgap, short wavelength, optoelectronics applications because of their exceptional physical properties. III-Nitrides have a direct bandgap which is tunable in energy from 6.2 eV (AlN), 3.4 eV (GaN) to 1.9 eV (InN) making them ideal for high efficiency photonic devices capable of operating from the ultraviolet (UV) to the red spectral regions. Such devices include UV-visible light emitting diodes (LEDs), laser diodes and solar-blind UV photodetectors for high density optical storage, high-brightness color displays, undersea and covert space-to-space communications and the detection of spacecraft above the ozone layer where there is a strong visible and infrared background.

Here, we report our progress for GaN thin films on sapphire substrates, followed by the growth and characterization of $Al_xGa_{1-x}N$ thin films on basal plane sapphire substrates in the entire compositional range, the n-type and p-type doping of $Al_xGa_{1-x}N$ as a function of alloy composition and dopant flow rate.

The thin films were grown using a horizontal low-pressure metalorganic chemical vapor deposition reactor (MOCVD). The 4 inch graphite susceptor was RF heated and spun at about 100 rpm to enhance the uniformity of the films. Trimethylaluminum (TMAl), trimethyl-(TMGa) and triethyl-gallium (TEGa) and ammonia (NH_3) were used as the source materials. Dilute silane (35 ppm SiH_4 in H_2) and dilute germane (50 ppm GeH_4 in H_2) were used as the n-type dopant sources, while biscyclopentadienylmagnesium (Cp_2Mg) was used as the p-type dopant source. Organometallic and hydride sources were separated until just before reaching the susceptor to minimize parasitic reactions. The carrier gas was a mixture of hydrogen and nitrogen. The growth temperature was 1000 °C. The films were grown on basal plane sapphire (Al_2O_3) substrates. A thin AlN or GaN buffer layer was first grown to improve the initial nucleation and enhance two dimensional growth.

The structural properties of the films were assessed through various techniques, including X-ray diffraction using a diffractometer operated in the "open detector mode", scanning electron microscopy (SEM) using a Hitachi S4500 field emission microscope. The optical and electrical

properties of the films were determined through optical transmission, photoluminescence using a 10 mW He-Cd laser and Hall effect measurements.

II.2. Progress for GaN thin films on (00•1) sapphire

Our previous work on the optimization of the MOCVD growth of GaN thin films has been reported earlier.[1] Since then, the material quality and the n-type and p-type doping of GaN on basal plane sapphire substrates have been further improved.

On the same wafer, GaN thin films exhibited at the same time mirror-like surface morphologies, narrow X-ray diffraction (30 arcsecs) and narrow room temperature and low temperature bandedge photoluminescence emission lines (e.g. 17 meV at 77K). This has also been achieved on wafer sizes up to two inches in diameter with good uniformity.

The n-type doping control of GaN using both silicon and germanium was achieved up to $n(300K)\sim10^{20}$ cm^{-3} and electron mobilities were increased to higher than 300 cm^2/Vs at room temperature. The p-type doping control was also improved and hole concentrations were increased to $1.2x10^{18}$ cm^{-3} at room temperature. Temperature dependent Hall effect measurements were carried out and yielded an activation energy of ~165 meV for the Mg dopant. This value is close to the value measured through temperature dependent photoluminescence.

II.3. Progress for $Al_xGa_{1-x}N$ thin films on (00•1) sapphire

The undoped $Al_xGa_{1-x}N$ thin films were grown on sapphire in the same growth conditions as for the GaN epilayers we reported earlier,[1] except that the Al source partial pressure in the reactor was varied. The films were about 1 μm thick as determined by SEM, corresponding to a growth rate of about 1 μm/hr. The samples were transparent with smooth surface morphologies, and they were insulating. The alloy composition was determined both by optical transmission and X-ray diffraction. However, the X-ray diffraction peak positions were shifted from their values for bulk films due to significant residual strain in the thin (00•1) $Al_xGa_{1-x}N$ films which resulted from a combination of lattice and thermal mismatch between the film and the Al_2O_3 substrate. [2] Therefore, optical transmission offered a better measure of the Al concentration than X-ray diffraction and this is the method we used in the rest of the report. Figure 1(a) shows typical optical transmission spectra of $Al_xGa_{1-x}N$, demonstrating that the entire ternary alloy composition is achieved. Figure 1(b) shows the x-ray rocking curve linewidths of the 00•2 diffraction peak for selected alloy compositions. The linewidths were lower than 4 arcmins for up to 50% Al, which represents the lowest values ever reported for such $Al_xGa_{1-x}N$ compounds. These linewidths are more than 10 times narrower than those reported in the literature.[3]

---

[1] P. Kung, A. Saxler, X. Zhang, D. Walker, T. C. Wang, I. Ferguson, and M. Razeghi, Appl. Phys. Lett. 66, 2958 (1995).

[2] K. Hiramatsu, T. Detchprohm, and I. Akasaki, Jpn. J. Appl. Phys. 32, 1528 (1993).

[3] T.J. Kistenmacher, D.K. Wickenden, M.E. Hawley, and R.P. Leavitt, Appl. Phys. Lett. 67, 3771 (1995).

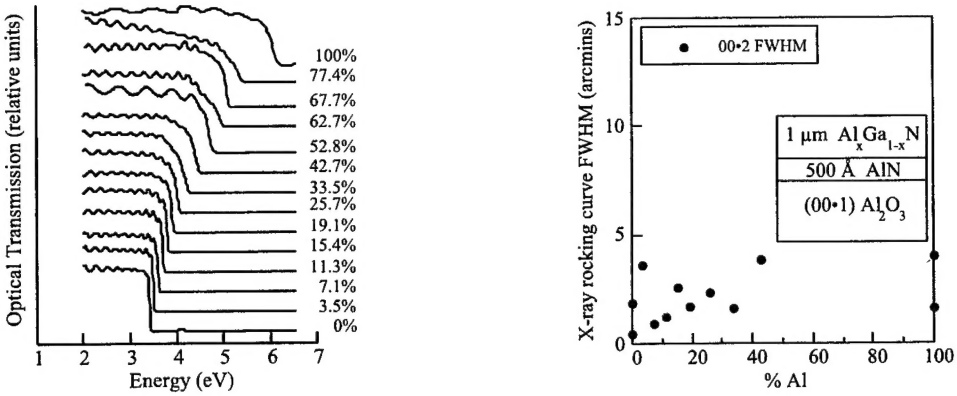

Figure 1. (a) Room temperature optical transmission spectra and (b) x-ray rocking curve linewidths of selected of $Al_xGa_{1-x}N$ thin films on sapphire substrates.

N-type and p-type doping of $Al_xGa_{1-x}N$ compounds was achieved by incorporating the dopant during the epitaxial growth. Doping was studied as a function of Al concentration and dopant flow rate. Figure 2(a) shows the resistivity, electron mobility and concentration in $Al_xGa_{1-x}N$ thin films doped with a fixed flow of SiH_4 as a function of alloy composition. It shows that the resistivity increases exponentially with Al concentration. The values for the resistivity were about 1 order of magnitude lower than those reported in the Ref. [4] and several orders lower than those reported in Ref. [5]. Mobilities as high as 80 cm^2/Vs were measured on $Al_{0.2}Ga_{0.8}N$:Si, which is the highest value ever reported for such a high Al concentration. The graph also shows that $Al_xGa_{1-x}N$ compounds can be n-type doped for an Al concentration higher than 50%, which is very promising for the realization of device structures with large band offsets using III-Nitride materials.

The n-type doping of $Al_{0.2}Ga_{0.8}N$ was studied as a function of SiH_4 and GeH_4 flow rates. The carrier concentrations increased linearly with dopant flow rate, up to $3x10^{19}$ cm^{-3}. The surface morphology of the films was not deteriorated by the doping in this range and the films were free from cracks.

Figure 2(b) shows the resistivity of $Al_xGa_{1-x}N$ thin films doped with a fixed flow of Cp_2Mg as a function of alloy composition. In order to activate the incorporated Mg, the samples were subjected to thermal annealing prior to any electrical measurement. Here again, the plot shows that the resistivity increases exponentially with Al concentration, from ~ 2 Ω.cm for GaN up to ~ 10^5 Ω.cm for $Al_{0.3}Ga_{0.7}N$.

[4] H. Murakami, T. Asahi, H. Amano, K. Hiramatsu, N. Sawaki, and I. Akasaki, J. Cryst. Growth 115, 648 (1991).
[5] S. Yoshida, S. Mizawa, and S. Gonda, J. Appl. Phys. 53, 6844 (1982).

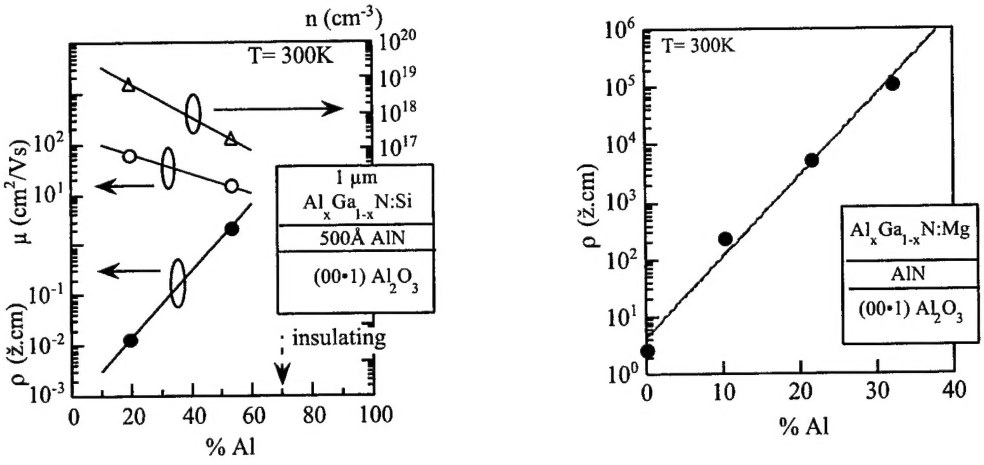

Figure 2. Room temperature (a) resistivity, electron mobility and concentration of Si-doped $Al_xGa_{1-x}N$ thin films; and (b) resistivity of Mg-doped $Al_xGa_{1-x}N$ thin films.

II.4. Comparison of trimethylgallium and triethylgallium for the growth of GaN

The choice of gallium precursors has recently been shown to influence the deep levels[6] and impurities[7] in GaN films. Here, we compare trimethylgallium (TMGa) and triethylgallium (TEGa) as gallium precursors for the metalorganic chemical vapor deposition (MOCVD) growth of GaN.

The GaN films were grown in a horizontal low-pressure (10 mbar) MOCVD reactor using a high temperature AlN buffer layer. Film thicknesses were typically about 0.7 µm. The organometallic gallium sources used were special grade TMGa, purified grade TMGa, and oxygen reduced grade TEGa from Morton, and adduct grade TEGa from Epichem. No significant differences were observed in the GaN layers as a function of the grade or supplier of these high purity organometallic sources. For purposes of comparison, the films were grown on identical (00·1) sapphire substrates, with identical AlN buffer layers, and with identical growth conditions except for the choice of the gallium source.

Figure 3 shows the (00·2) GaN open-detector x-ray diffraction rocking curves for samples grown using TMGa and TEGa. The full width at half maximum (FWHM) for the TEGa grown film was 33 arcseconds while the TMGa grown film had a FWHM of 62 arcseconds. The linewidth and tails were somewhat narrower for the film grown using TEGa. Pendellösung oscillations for the TEGa grown film are visible even in the open-detector rocking curve shown in Figure 3(b).

---

[6] J.-F. Chen, N.-C. Chen, W.-Y. Huang, W.-I. Lee, and M.-S. Feng, *Jpn. J. Appl. Phys.* 35, L810 (1996).
[7] A. Ishibashi, H. Takeishi, M. Mannoh, Y. Yabuuchi, and Y. Ban, *J. Electron. Mater.* 25, 799 (1996).

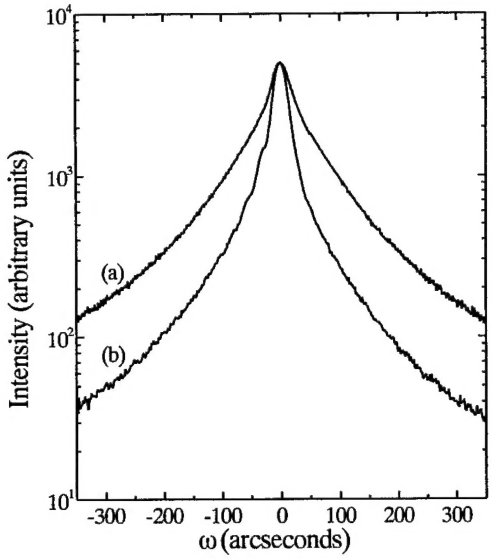

Figure 3. Open-detector x-ray rocking curves of the (00·2) GaN peak of (a) a sample grown with TMGa and (b) a sample grown with TEGa under otherwise identical growth conditions.

Figure 4 shows the room temperature photoluminescence (PL) spectra measured using a 325 nm He-Cd laser for samples grown using TMGa and TEGa. Typically, the near bandgap luminescence was much stronger for the samples grown using TEGa, although the yellow luminescence was approximately the same as illustrated in Figure 4. From these results, it is clear that the films grown using TEGa have better optical quality than films grown using TMGa.

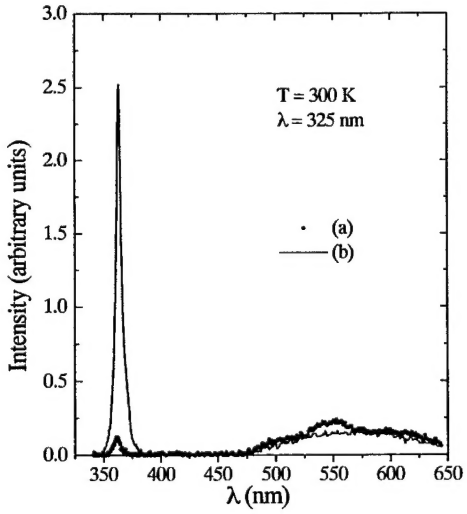

Figure 4. Room temperature photoluminescence spectra of (a) a sample grown with TMGa and (b) a sample grown with TEGa under otherwise identical growth conditions.

Figure 5(a) shows the variation of the electron mobility and carrier concentration as a function of the dopant flow rate of dilute SiH_4 for GaN films grown using TMGa and TEGa. The mobility of TEGa grown films was typically much higher than in TMGa grown films as seen in the figure. Undoped films were typically insulating (> ~10^8 Ω cm) for films grown using

either TMGa or TEGa. The TMGa grown films required a flow rate of 20 sccm dilute SiH4 in order to achieve conduction, and the resulting mobility was extremely low indicating that the TMGa grown films are heavily compensated. The TEGa grown films were easier to dope and had higher mobilities as seen in Figure 5(a).

Figure 5(b) shows the secondary ion mass spectroscopy (SIMS) depth profiles for typical samples grown using TMGa and TEGa using cesium for the primary ions. At a depth of about 400 nm, the oxygen concentration was 7 times higher, and the carbon concentration was 50 times higher in the TMGa grown film compared to the TEGa grown film. The higher concentration of carbon and oxygen in the GaN layers grown using TMGa may be responsible for the poorer electrical and optical properties of those films.

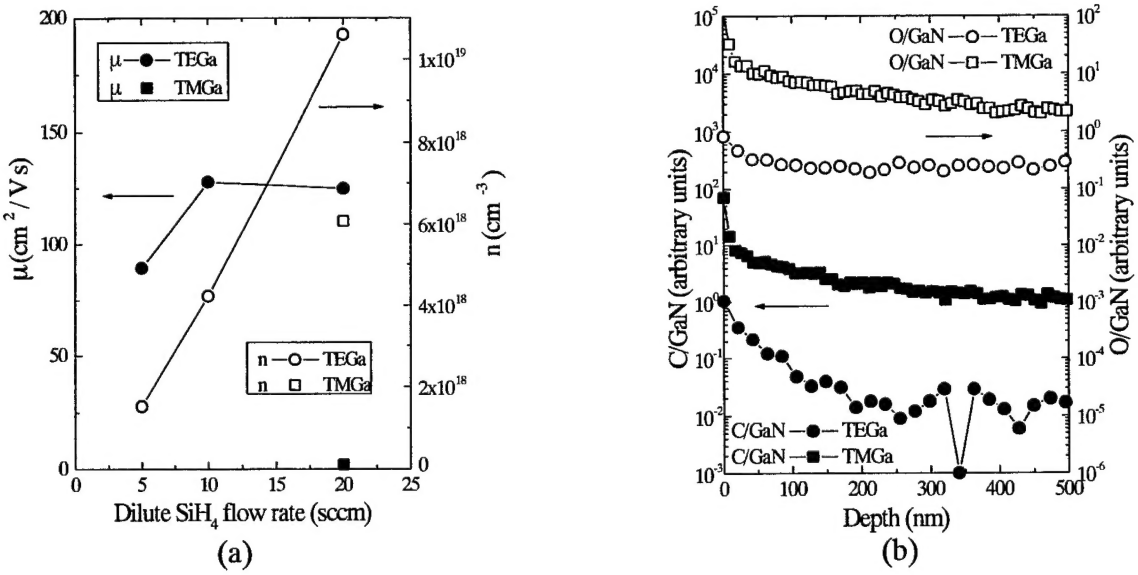

Figure 5. (a) Room temperature electron mobility and n-type carrier concentration for TMGa and TEGa grown samples as a function of the doping level using otherwise identical growth conditions. (b) SIMS depth profiles of oxygen and carbon normalized to the GaN signal in a sample grown with TMGa and a sample grown with TEGa under otherwise identical growth conditions.

In order to further assess the material quality, hot phosphoric acid (H_3PO_4) was used to attack the GaN films. A scanning electron microscope (SEM) with a field emission gun was used to examine the surface.

The etch pits in the GaN films exhibited hexagonal symmetry as seen in Figure 6. The bases of the hexagons were determined to be along the [[11·0]] directions through x-ray diffraction measurements. The walls appear to be nearly vertical, so the etched faces correspond to the {10·0} planes. The etch pit density (EPD) was approximately 10^4 cm^{-2} for these films. The typical size of the etch pits ranged from 2 to 40 μm. (This EPD compares favorably with an

EPD of over 10^7 cm^{-2} that was revealed in early GaN films by Shintani and Minagawa with this etching technique.[8])

Although the density of these large etch pits was approximately equal in the films grown using TMGa and TEGa, the borders were very different. The TEGa grown film had sharp borders as seen in Figure 6(b). The TMGa grown film had irregular borders as seen in Figure 6(a). In addition to these large pits with a density of 10^4 cm^{-2} in the TMGa grown film, smaller pits were present with a density of 10^9 cm^{-2} and sizes of about 0.05 to 0.1 μm. It is possible that when these small pits are present near the edge of the large pits, the border extends to envelop them, creating an irregular border. None of these small pits were present in the TEGa grown film that was grown under identical conditions. It is possible that the difference in the shape of the etch pits for TMGa grown films is due to the higher carbon and oxygen impurity concentration which enhances the etching rate in the vicinity of defects.

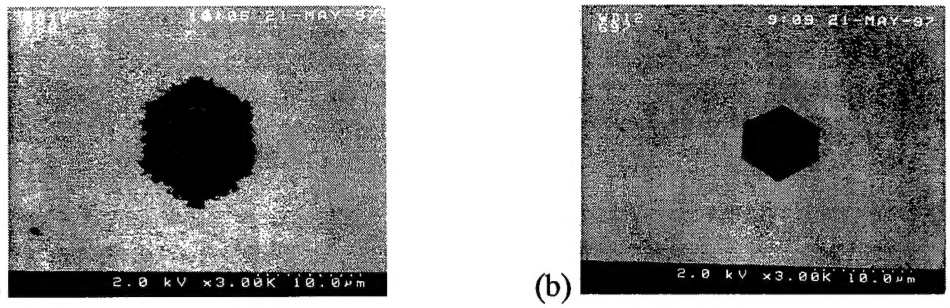

Figure 6. SEM images of hexagonal etch pits in GaN in (a) a sample grown using TMGa and (b) a sample grown using TEGa under otherwise identical growth conditions. The TEGa grown sample has etch pits with sharp edges while the TMGa grown sample has etch pits with rough edges.

In summary, films grown using TEGa showed stronger near-bandedge photoluminescence, higher mobilities, and lower impurity concentrations than films grown using TMGa. Hot phosphoric acid was used to measure the EPD to be 10^4 cm^{-2} for large pits in films grown with either TMGa or TEGa. The edges of the large etch pits in the TEGa grown films were generally sharp while the borders of the etch pits in the TMGa grown films were irregular. The TMGa film also had small pits with a density of 10^9 cm^{-2} which were not present in the TEGa grown film. SIMS measurements indicated higher carbon and oxygen concentrations in the films grown using TMGa. We conclude that TEGa is the superior gallium source for the MOCVD growth of GaN for the experimental conditions studied.

[8] A. Shintani and S. Minagawa, *J. Electrochem. Soc.* 123, 706 (1976).

III. SCHOTTKY MSM ULTRAVIOLET PHOTODETECTORS

III.1. Introduction

Gallium nitride has been the focus of intense interest in recent years due to advances in crystal growth technology and device fabrication procedures. Its direct, wide band gap makes it an ideal choice for use in various detector applications such as ultraviolet (UV) astronomy, flame detection and engine monitoring, where harsh working environments exploit the natural durability and visible-blindness of the material.[9]

Several groups have reported the characterization of photoconductive and photovoltaic p-i-n nitride-based photodetectors. GaN Schottky barrier devices have been shown to have high speed and low noise capabilities.[10] In contrast, much less work has been published concerning Schottky-based metal-semiconductor-metal (MSM) photodetectors. These devices consist of two Schottky contacts on a planar surface. GaN MSM detectors with very low dark currents have been demonstrated, but no information about the speed was provided.[11] In this work, we report the fabrication and characterization of high speed GaN and GaN:Mg MSM photodetectors with sharp wavelength cut-off and high ratio of rejection of visible light to ultraviolet light.

III.2. Experiment

GaN:Mg and non-intentionally doped (n.i.d.) GaN layers were grown by low-pressure metalorganic chemical vapor deposition on basal plane sapphire. The details of the crystal growth have been reported previously. Low resistivity p-type GaN was achieved in the Mg doped sample after exposure to rapid thermal annealing in an N_2 ambient environment. The interdigitated Pt/Au Schottky contacts were deposited by electron-beam evaporation. The fingers were 150 μm long and 2μm wide with a pitch of 10 μm, as seen in Figure 7.

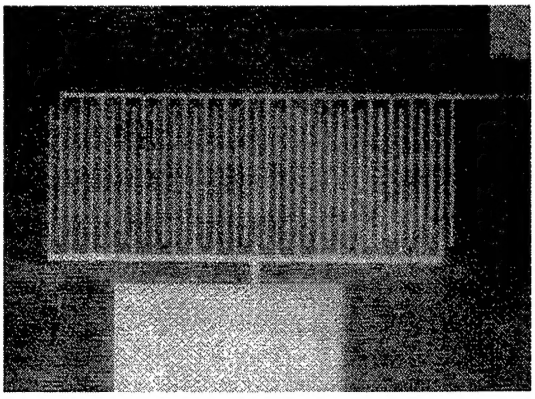

Figure 7. Top view of MSM device showing interdigitated geometry. Finger width is 2 μm, length is 150 μm, and pitch is 10 μm.

---

[9] M. Razeghi and A. Rogalski, J. Appl. Phys. 79, 7433 (1996).

[10] Q. Chen, J. W. Yang, A. Osinsky, S. Gangopadhyay, B. Lim, M. Z. Anwar, M. A. Khan, D. Kuksenkov, and H. Temkin, Appl. Phys. Lett. 70, 2277 (1997).

[11] J. C. Carrano, T. Li, P. A Grudowski, C. J. Eiting, R. D. Dupuis, and J. C. Campbell, J. Appl. Phys. 83, 6148 (1998).

III.3. Photodetector characterization and discussion

In order to study the quality of the Schottky barriers, an indium ohmic contact was deposited near the edge of the sample. The current-voltage (I-V) characteristics measured between the ohmic and Schottky contacts are displayed in the inset of Figure 8.

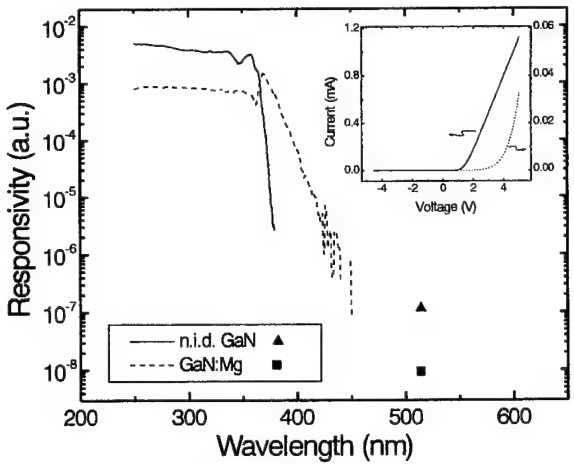

Figure 8. Spectral response of the n.i.d. GaN and GaN:Mg MSM photodetectors. In the inset, the I-V characterization of the Schottky contacts.

They show an ideality factor of ~1.5 and ~4, for n.i.d. GaN and GaN:Mg respectively, with leakage resistances >10GΩ. The dark current value for the GaN:Mg MSM detector is ~12 nA at 5 V and is only ~2nA at 5 V for the GaN MSM device, which is additional confirmation of the high quality of the contacts as well as the material.

A Xe arc lamp was used as the optical source for the spectral responsivity studies and a standard synchronous detection scheme was employed to measure the front-side-illuminated detector signal. The system was calibrated with a UV-enhanced Si detector. The responsivity dependence on optical power was determined by excitation with a cw He-Cd laser (325 nm). The response time of the detectors was measured using a pulsed nitrogen laser (337 nm) as the optical source. Noise characterization was performed using a SR760 FFT spectrum analyzer with the devices connected to a Keithley 428 current amplifier, so that the background noise power density of the system is about 10^{-24} A^2/Hz.

The spectral response for the n.i.d GaN and GaN:Mg MSM detectors are shown in Figure 8. The most striking difference between these two response curves is the slope of the wavelength cut-off. The response of the GaN MSM detector shows a very abrupt cut-off, whereas the GaN:Mg MSM detector has a more gradual decline at longer wavelengths. This slight absorption of photons with energy below the bandgap is due to the presence of Mg related levels in the material. Using the measurement setup described above, it was not possible to detect any photogenerated signal for wavelengths longer than 400 nm. Therefore, an Ar laser (514 nm) was used to obtain a photoresponse in the visible spectral region, also displayed in Figure 8. Both response curves exhibit high visible rejection, with an ultraviolet/green contrast of about five orders of magnitude. This measurement at higher power levels (Ar laser) was

justified in the next series of experiments, which showed that the responsivity is constant over the power range utilized.

The photocurrent increases linearly with the optical power for the GaN:Mg device as seen in Figure 9, and shows no saturation at higher power levels. The n.i.d. GaN device, however, follows a P^k fit, where P is the optical power and k=0.9, which is a much better result than the k=0.1 behavior reported for n.i.d. GaN photoconductors.[12] To investigate the possibility of an internal gain mechanism, the responsivity was measured with respect to the voltage bias. The results of this test are seen in the inset of Figure 9.

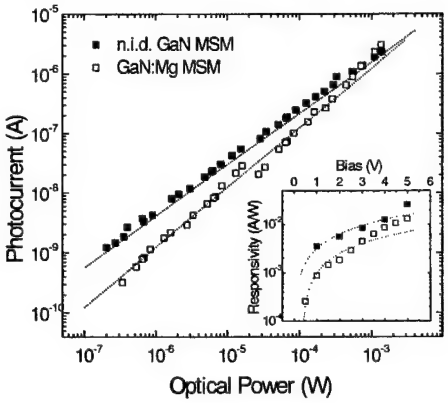

Figure 9. The photocurrent dependence on optical power for n.i.d. GaN and GaN:Mg MSM photodetectors, measured with the He-Cd laser (325 nm). In the inset, the scaling of the responses with increasing bias voltage.

Both the n.i.d. GaN and the GaN:Mg MSM devices exhibited a scaling of the responsivity with voltage bias. This increase indicates the presence of an internal gain mechanism such as hole trapping. The shape of the spectral response has been found to be independent of bias up to 5 V.

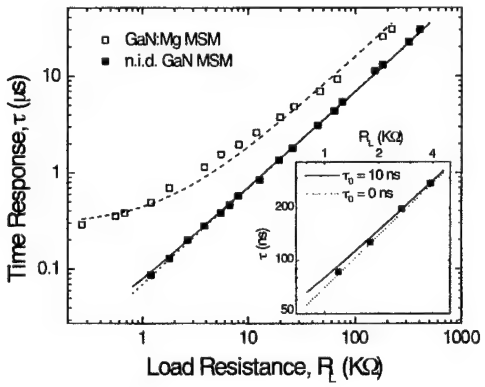

Figure 10. Photocurrent decays measured with a pulsed nitrogen laser for different load resistances. In the inset, the magnification of low load data, showing the divergence of the 10 ns and 0 ns linear fits.

---

[12] E. Muñoz, E. Monroy, J.A. Garrido, I. Izpura, F.J. Sánchez, M.A. Sánchez-García, and E. Calleja, B. Beaumont, and P. Gibart, Appl. Phys. Lett. 71, 870 (1997).

The temporal response of these devices shows no persistent photoconductivity. The dependence of photocurrent response time on load resistance has been analyzed to acquire the minimum time response of the detector, and is seen in Figure 10.

The photocurrent decays are exponential for the n.i.d. GaN MSM device. The GaN:Mg device shows exponential decays for high load resistances (>50 kΩ), but they become non-exponential for lower load resistances and tends towards a response time of 200 ns, as shown in Figure 10. In the exponential regimes the time constant is limited by the RC product of the system, where R is the load resistance and C is the sum of the capacitance of the device and the load capacitance of our measurement system. In order to estimate the minimum time response of the n.i.d. GaN MSM detector, the decay time constants are plotted as a function of the load resistance. In order to find the real speed limitation of the device, this data is fitted to linear functions with zero-load time constants of 10 ns and 0 ns (straight and dotted lines in Figure 10). From the magnified view of the low load data, shown in the insert, it is clear that this measurement provides the precision only to attest that the time response lies below 10 ns.

The noise analysis for the detectors was preformed at biases up to 5 V. For the GaN:Mg MSM device the only differentiation from the background noise of the system was seen at 5 V, as shown in Figure 11. The noise power density exhibited a 1/f dependence, which is expected for this wide bandgap material. The noise power density of the n.i.d. GaN MSM device remained below the background level, even when biased at 5 V.

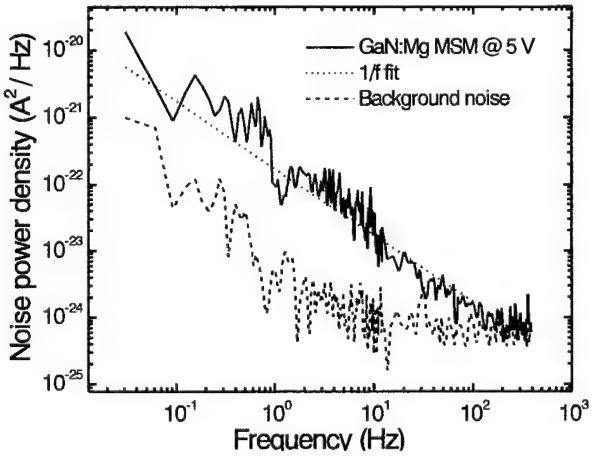

Figure 11. Noise power density spectrum of GaN:Mg MSM photodetector and the background noise level.

III.4. Summary

In summary, we report the fabrication and characterization of n.i.d. GaN and GaN:Mg MSM photodetectors, with high speed and visible rejection. Photocurrent decays are exponential for the n.i.d. GaN device and for high load resistances with the Mg doped device, with time constants corresponding to the RC product of the system. Minimum response times are <10 ns and about 200 ns for the for the n.i.d. GaN and GaN:Mg MSM devices, respectively. The noise power spectral density remains below the background level of the system (10^{-24} A^2/Hz) up to 5V for the n.i.d. GaN MSM detector.

IV. GAN P-I-N PHOTODIODES WITH HIGH VISIBLE-TO-ULTRAVIOLET REJECTION RATIO

IV.1. Introduction

Recent technological advances in III-Nitride semiconductors, and in $Al_xGa_{1-x}N$ materials in particular, have renewed the interest and led to significant progress in ultraviolet (UV) photodetectors based on these materials. There have been a growing number of applications which require the use of such sensors, which are able to detect light in the mid- and near-UV spectral region corresponding to a short wavelength, between 200 and 400 nm. Examples of such applications include UV astronomy, flame detection, furnace control, engine monitoring, water purification, UV radiation dosimetry, pollution monitoring, early missile threat warning, chemical/biological battlefield reagent detectors, and space-to-space communications.[13,14,15]

In many of these applications, it is important to detect ultraviolet light without also detecting infrared or visible light, especially from the Sun, in order to minimize the chances of false detection or high background. This property is often called the visible blindness of the detector. Because most applications are airborne or are in spacecraft, it is important to achieve the most lightweight and simplest photodetector possible. III-Nitride materials, GaN and $Al_xGa_{1-x}N$ compounds, are the most suitable candidate for such applications. First, they have a direct wide bandgap ranging continuously from 200 to 365 nm. Another consequence of their wide bandgap is the intrinsic solar-blindness and low dark currents. III-Nitride detectors would therefore not need Wood's filters to eliminate longer wavelengths as silicon detectors do, thus reducing cost and launch weight.[14,15] Moreover, III-Nitrides are both physically and chemically strong, which makes them ideal for radiation-intense space applications and less subject to ageing. Finally, a wider bandgap results in lower dark currents. III-Nitride photodetectors would therefore not need heavy cooling systems.

To date, most of the work on III-nitride UV photodetectors has been conducted to prove the potential of III-Nitride materials for UV photodetector applications.[16,17,18] Typical values of UV-to-visible rejection ratio, which is the ratio of the photoresponse of UV light to the photoresponse of visible light, have been about 3 to 4 orders of magnitude for GaN photoconductors.[19] Very limited work has been devoted to characterizing or improving this ratio. We here report the growth and characterization of GaN p-i-n photodiodes on basal plane

---

[13] M. Razeghi and A. Rogalski, *J. Appl. Phys.* 79(10), 7433-7473 (1996).

[14] M.P. Ulmer, M. Razeghi, and E. Bigan, *Optoelectronic Integrated Circuit Materials, Physics, and Devices*, SPIE Proc. vol. 2397, eds. M. Razeghi, Y.S. Park and G.L. Witt, 210-217 (SPIE Optical Engineering Press, Bellingham, 1995).

[15] A. Rogalski and M. Razeghi, *Opto-Electr. Rev.* 4, No. 1/2, 13-30 (1996).

[16] D. Walker, X. Zhang, A. Saxler, P. Kung, J. Xu, and M. Razeghi, *Appl. Phys. Lett.* 70 (8), 949-951 (1997).

[17] M.A. Khan, J.N. Kuznia, D.T. Olson, M. Blasinghame, and A.R. Bhattarai, *Appl. Phys. Lett.* 63(18), 2455-2457 (1993).

[18] P. Kung, X. Zhang, D. Walker, A. Saxler, J. Piotrowski, A. Rogalski, and M. Razeghi, *Appl. Phys. Lett.* 67(25), 3792-3794 (1995).

[19] C.H. Qiu and J.I. Pankove, *Appl. Phys. Lett.* 70(15), 1983-1985 (1997).

sapphire substrates with a visible-to-UV light rejection ratio of 6 orders of magnitude, which is the highest value ever reported.

IV.2. Material growth and characterization

The GaN p-i-n photodiode structure studied is shown in Figure 12. It consists of a 1 μm n-type Si-doped GaN layer, followed by a 1000 Å undoped GaN layer, and terminated by a 2000 Å Mg-doped GaN layer.

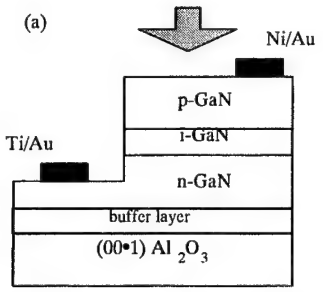

Figure 12. Schematic of a typical photodiode mesa structure.

After epitaxial growth, the samples were annealed using a rapid thermal annealer to achieve low-resistivity p-type GaN:Mg. The surface of the sample was partially removed using ECR-RF dry etching until the n-type GaN was exposed to form 400μm × 400μm square mesa structures. Ni/Au and Ti/Au metals were evaporated onto the p-type and n-type GaN respectively, using an electron-beam evaporator. Gold wires were used to contact the mesas. Individual n-type and p-type GaN films have been optically and electrically characterized through conventional room temperature photoluminescence using a He-Cd laser as the excitation source (325nm, ~10mW) and Hall measurements. The spectral responsivity of the photodiodes was measured using a Xe arc lamp, a monochromator, an optical chopper, and a lock-in amplifier in a synchronous detection scheme. The sample was uniformly illuminated from the front side. To obtain the absolute spectral responsivity, the power of the Xe lamp as a function of wavelength was factored out. This was done using a calibrated Si detector that was first used in place of the tested photodiode to measure the Xe lamp spectrum. The responsivity and photocurrent were measured with respect to the input optical power at room temperature, using the He-Cd laser as the excitation source for both 0 and –5 V bias. For temporal response measurements, the photodiode was connected to a Keithley 428 current amplifier with a maximum voltage bias of ±5V, alternately using a He-Cd laser and a nitrogen laser as excitation sources.

Figure 13(a) shows the room temperature photoluminescence spectrum from a typical GaN:Si thin film grown in the same conditions as used for the p-i-n photodiode. A sharp peak was observed at 364 nm near the band-edge emission of GaN:Si. Negligible deep level luminescence could be observed at longer wavelengths. Hall measurements yielded a room temperature carrier mobility and concentration of ~230 cm^2/Vs and $5x10^{18}$ cm^{-3} for a 1 μm-thick GaN:Si test film. Figure 13(b) illustrates the room temperature photoluminescence spectrum from a typical GaN:Mg thin film after the RTA process. Only a broad peak around 425 nm could be observed. At room temperature, the films showed p-type conductivity with free hole

mobility and concentrations of ~10 cm^2/Vs and $1x10^{17}$ cm^{-3}, respectively, for 1 μm-thick GaN:Mg films.

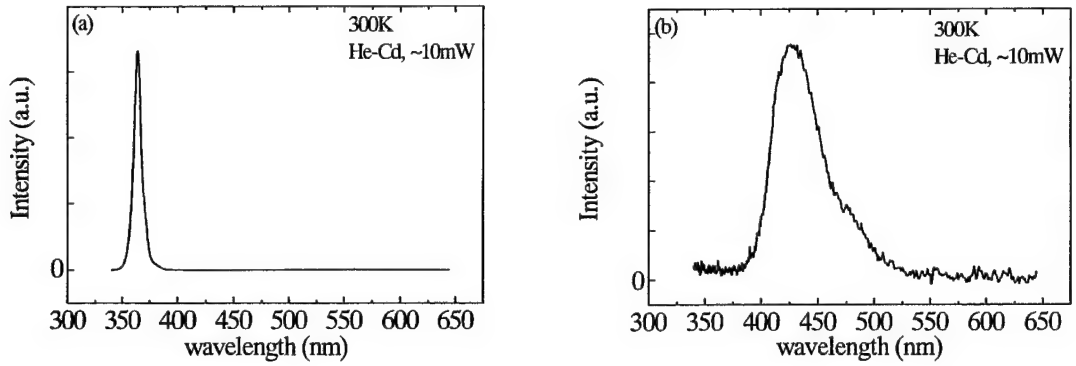

Figure 13. Room temperature photoluminescence spectra from (a) n-type GaN:Si and (b) p-type GaN:Mg layer.

IV.3. Photodetector characterization and discussion

The absolute spectral responsivity of the GaN p-i-n photodiode without bias is plotted in Figure 14 (solid line). The device area used in the calculations was the exposed surface area of the mesa ($400\mu m^2$-$150\mu m^2$). The responsivity was nearly constant below ~365 nm. A peak responsivity of 0.15 A/W at 363 nm was achieved. The theoretical current responsivity for a p-i-n photodiode is given by

$$\textit{Equation 1.} \qquad R_I(\lambda) = \frac{q\lambda}{hc}\eta$$

where λ is the photon wavelength and η is the external quantum efficiency.[20] This external quantum efficiency includes the internal quantum efficiency and reflectivity losses. Using the value obtained for the responsivity at 363 nm, an external quantum efficiency of η~0.51 is estimated for our p-i-n photodiodes.

Using the measurement setup described above, it was not possible to detect any photogenerated signal for wavelengths longer than about 390 nm. A high power argon laser (514 nm) was then used to obtain a photoresponse in the visible spectral region and the value of the responsivity is shown in Figure 14 as a triangle. By dividing the values of the responsivity at 363 nm and at 514 nm, a value of 10^6 was obtained for the UV-to-visible rejection ratio, which is about three orders of magnitude higher than other reports on III-Nitride based UV photodetectors.[19] This represents a major step for the future application of III-Nitride based UV photodetectors, in particular for UV astronomy where a rejection ratio much higher than 10^4 is needed.[14] Because GaN has a wide bandgap, crystal defects or impurities in the material may easily create energy levels within the gap. These levels form recombination centers that harm the performance of UV photodetectors, in particular their visible blindness. The improvement of

[20] A. Rogalski, *Infrared Photon Detectors*, 35,51 (SPIE Optical Engineering Press, Bellingham, 1995).

the visible blindness for our GaN based UV detectors can be partly attributed to better control of the material growth technology (reduction of impurity and defect densities). Further improvements in rejection ratio may be achieved by optimizing the device geometry and structure design.

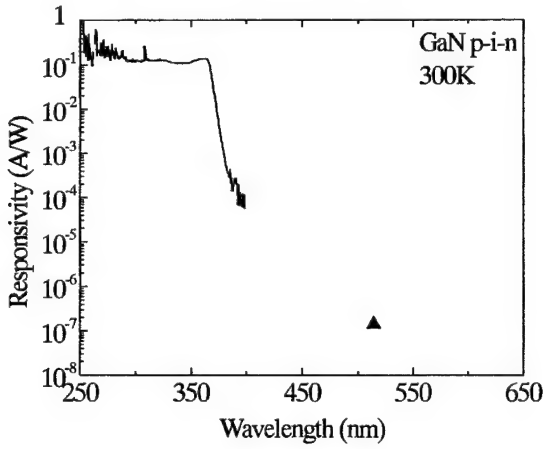

Figure 14. Room temperature spectral response of a typical GaN p-i-n photodiode.

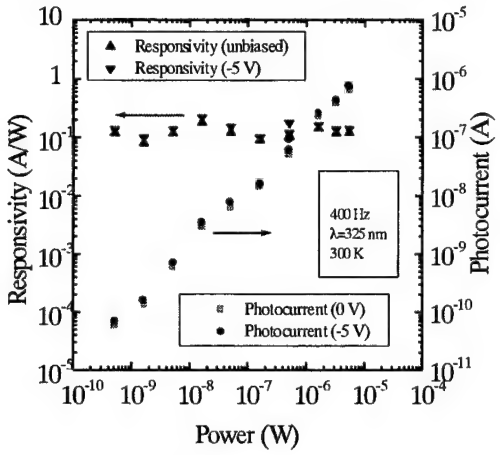

Figure 15. Responsivity and photocurrent measured with increasing optical power.

Figure 15 shows the resulting responsivity and photocurrent of the photodiode for optical power levels over many orders of magnitude. The photocurrent increases linearly for increasing power which yields a constant responsivity value.

The current-voltage curve of one of these diodes is shown in the inset of Figure 16. The current at reverse bias is three orders of magnitude less than the current for the same voltage at forward bias. The resistance plotted with respect to bias voltage, as seen in Figure 16, indicates the turn on voltage at ~3V with a dramatic decrease in resistance of seven orders of magnitude. This plot also shows the zero bias resistance of $10^{11}\Omega$. This high zero bias resistance ensures that the Johnson noise level will be low.

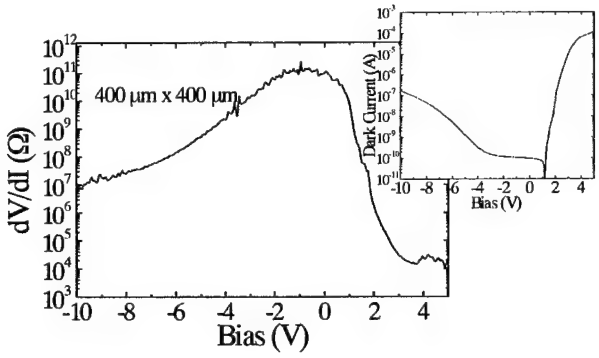

Figure 16. Room temperature resistance-and current-voltage curves of a p-i-n photodiode.

The rise and fall times, which indicate at what speed a device is able to operate, are examined for various bias voltages. The square wave of period 250 μs is created by the optical chopper spinning at a frequency of 4kHz. The beam from a He-Cd laser (325 nm) is focused at the plane of the chopper so that any slope in rise time and fall time due to the partial blocking of the beam by the chopper as it rotates is minimized, although this effect cannot be entirely removed because of the finite size of our focused beam. Another limitation is found in the current amplifier itself, which contributes a rise and fall time of 5 μs for a gain of 10^6. As seen in Figure 17, as the negative bias is increased from 0 to -5 volts the response of the diode is noticeably faster. Both the rise and fall times respond to the higher negative bias and attain the switched level more quickly than their lower biased counterparts. A more accurate estimate of the rise and fall times for this detector was taken with a pulsed nitrogen laser as the optical source so that a chopper and current amplifier, which introduce additional response delays to the measurement, would not be necessary. Figure 18 shows a fall time speed of the photodiode of about 2.5 μsec. This response time, although not as limited as if using the previous setup, is believed to still be limited by the measurement apparatus. The increase in response speed with an increase in voltage bias, as seen in Figure 17, suggests that the speed of these GaN p-i-n photodiodes is limited by the RC time constant of the detection circuit, where R is the total resistance and C is mainly the capacitance of the depletion layer in the diode. Indeed, the RC time constant can be reduced by increasing the reverse bias, which extends the depletion layer, and thus reduces the capacitance C. A rough estimate of the RC time constant yields a value of τ_{RC}~1.4 μs, assuming the following parameters for GaN: R~1× $10^4\Omega$, $\varepsilon = 10.4\varepsilon_0$ (E//c); W=0.1 μm and A=(400 μm)^2 for the width and area of the depletion layer respectively. This value of τ_{RC} is on the same order as our estimate of the response speed from Figure 18. Further work is in progress to improve the speed performance of GaN p-i-n photodiodes by optimizing the device geometry and structure design, and the ohmic metal contacts.

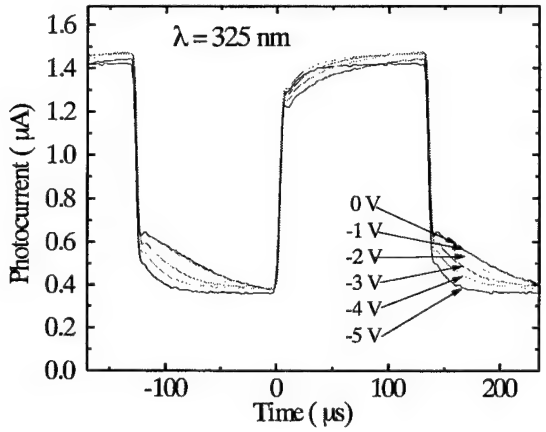

Figure 17. The temporal response display of rise and fall times for various voltage biases.

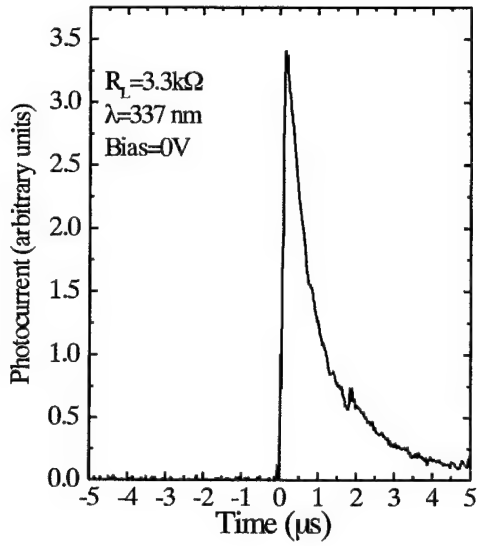

Figure 18. The temporal response with a pulsed nitrogen laser as the optical source.

IV.4. Summary

In summary, GaN p-i-n photodiodes were grown by low-pressure MOCVD , which exhibit a UV-to-visible rejection ratio of 6 orders of magnitude. Measurements of the temporal response, which appears to be RC limited, indicate a response time of 2.5 μs. These diodes have a zero bias resistance of 10^{11} Ω, and an absolute responsivity of 0.15 A/W at 363 nm. This is very promising for the commercial applications of III-Nitride UV photodetectors.

V. ANALYTICAL MODELING OF GAN P-I-N PHOTODIODE

V.1. Analytical modeling of GaN p-i-n photodiode

In the development of photonic devices, such as ultraviolet photodetectors, it is important to use the details of the detector characterization to understand the material properties more thoroughly. This helps in the design of more effective diodes providing design constraints such as an optimum thickness for the absorbing layer. The analysis of the device data also aids in the further understanding of the semiconductor material properties, leading to improved growth and processing techniques. Although, Analytical modeling of AlGaN photodetector devices is of main interest but is not possible since many of material parameters needed for this purpose are not yet known. As the first step toward understanding the material properties of this class of devices, analytical modeling of the responsivity of a GaN p-i-n photodetector was performed because many material related parameters are known (e.g. m_h, m_e, D_h, etc.). Using a simple partial modeling of GaN p-i-n photodiodes, a hole diffusion length of 1000 Å was obtained as indicated in a previous study.[21] The analytical modeling of GaN p-i-n photodetectors has lead to the first experimental determination of the minority carrier diffusion length in p-GaN. This information, coupled with further experimental analysis of higher Al content ternary devices, will allow the extrapolation of the minority carrier diffusion length in AlGaN solar blind photodetectors.

V.2. Literature Survey

Optimization of operation of visible blind UV photodetectors (especially of interest the solar blind AlGaN photodetectors) is possible through understanding of fundamental material properties. Minority carrier diffusion lengths and lifetimes are critical in device performance. Larger minority electron diffusion length in solar blind AlGaN photodetectors ensures highly efficient absorbance of the incident light by the intrinsic region resulting in a high responsivity and quantum efficiency. Determination of minority electron diffusion length in p-GaN has been previously reported.[2223] An electron diffusion length of 2000 Å was reported through the measurement of electron beam induced current in p-GaN material.[2] This is the only experiment that has directly measured the minority electron diffusion length in p-GaN. Analysis of external quantum efficiency of GaN homojunction photodetector has been also reported to result in a minority electron diffusion length of only 250 Å.[3] It was speculated that this low value is due to the existence of a dead layer underneath the p-GaN surface that does not contribute to the collection of photogenerated carriers. We have recently reported an electron diffusion length of about 880 Å through modeling of the spectral responsivity of GaN p-i-n photodiodes using a calculation for the quantum efficiency.[24] Although, this value is still smaller than 2000 Å but it shows relatively high quality p-GaN material.

---

[21] X. Zhang, P.Kung, D. Walker, J. Pietrowski, A. Rogalski, A. Saxler, and M. Razeghi, *Appl. Phys. Lett.* 67, 2028 (1995).

[22] Z. Z. Bandic, P.M. Bridger, E. C. Piqutte, and T. C. McGill, *Appl. Phys. Lett.* 73, 3276 (1998)

[23] Ting Li, J. C. Carrano, J. C. Campbell, M. Schurman, and I. Ferguson, *IEEE J. Quantum Elect.* 35, 1203 (1999)

[24] D. Walker, P. Sandvik, P. Kung, V. Kumar, F. Shahedipour, K. Mi, and M. Razeghi, Submitted to the *Appl. Phys. Lett.*

V.3. Determination of minority carrier diffusion length in p-GaN

The spectral responsivity for the GaN p-i-n photodiode was modeled using calculations for the quantum efficiency in each of the three bulk regions of the device, the p, i and n:

Equation 2.
$$\eta_p := \frac{(1-r)\cdot\alpha\cdot L_e}{(\alpha)^2\cdot L_e{}^2 - 1}\cdot\left[\frac{\alpha\cdot L_e + \gamma_1 - \exp(\alpha\cdot x)\cdot\left(\gamma_1\cdot\cosh\left(\frac{x}{L_e}\right) + \sinh\left(\frac{x}{L_e}\right)\right)}{\gamma_1\cdot\sinh\left(\frac{x}{L_e}\right) + \cosh\left(\frac{x}{L_e}\right)} - \alpha\cdot L_e\cdot\exp(-\alpha\cdot x)\right]$$

Equation 3.
$$\eta_n := \frac{(1-r)\cdot\alpha\cdot L_h}{(\alpha)^2\cdot L_h{}^2 - 1}\cdot\exp(-\alpha\cdot(x+w))\cdot\frac{\left(\gamma_2 - \alpha\cdot L_h\right)\cdot\exp(-\alpha\cdot t) - \sinh\left(\frac{t}{L_h}\right) - \gamma_2\cdot\cosh\left(\frac{t}{L_h}\right)}{\cosh\left(\frac{t}{L_h}\right) - \gamma_2\cdot\sinh\left(\frac{t}{L_h}\right)} + \alpha\cdot L_h$$

Equation 4.
$$\eta_i := (1-r)\cdot(\exp(-\alpha\cdot x) - \exp(-\alpha\cdot(x+w)))$$

where x, w and t are the thickness of p, i, and n regions (cm), respectively; L_e and L_h are the minority carrier diffusion lengths (cm); μ_n, μ_p are the mobilities (cm^2/Vs) of each doped region; and D_e and D_h are the minority carrier diffusion coefficients.

The total quantum efficiency of the device is the sum of the efficiency in each of the three regions:

Equation 5.
$$\eta := \eta_p + \eta_n + \eta_i$$

and the responsivity is found using the basic relationship:

Equation 6.
$$Resp := \frac{q\cdot\eta\cdot\lambda}{h\cdot c}$$

The GaN layers were grown by low-pressure metal-organic chemical vapor deposition on basal plane sapphire. Growth details have been reported previously. Rapid thermal annealing was used to activate the Mg-doped GaN layer prior to any device fabrication. Based on the small absorption length expected in p-GaN, the p-GaN layer ($N_A = 1.5\times10^{17}$ cm^{-3}) was grown only 1000 Å thick. The 2000 Å thick unintentionally-doped intrinsic layer ($N_D = 1.7\times10^{16}$ cm^{-3}) is sufficiently thick to absorb much of the incident light. Very few photons are expected to reach the relatively thick n-type layer ($N_D = 1.5\times10^{18}$ cm^{-3}).

From a fit of the standard equation for spectral responsivity, using a hole diffusion length of 1000 Å as indicated by previous studies[1] and absorption spectra obtained from transmission measurements, the electron diffusion length in the p-GaN material was found to be 880 Å. The spectral responsivity of the GaN p-i-n photodiode and the theoretical fit are shown in Figure 19.

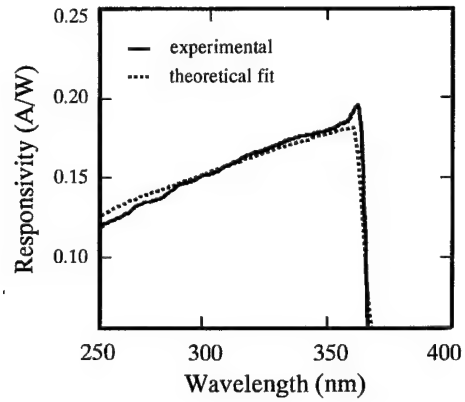

Figure 19. The spectral responsivity of the GaN p-i-n photodiode and the theoretical fit.

The response peak in the experimental data at the bandedge is due to excitonic effects, which are not considered in the model. The electron diffusion length found seems short compared to a previous report of 2000 Å, but several recombination mechanisms are responsible for an observed diffusion length indicating that material properties greatly influence this measurement.

V.4. Summary

In summary, the analytic modeling of the responsivity for a GaN p-i-n photodiode allowed the extraction of the minority carrier diffusion length for electrons in the p-type GaN material. This was found to be 880Å, which was close to the thickness of the p-layer. This fortunate design choice enabled this device to attain 86% internal quantum efficiency.

VI. VISIBLE AND SOLAR BLIND $AL_XGA_{1-X}N$ ULTRAVIOLET P-I-N PHOTODIODES

VI.1. Introduction

The successes in the realization of GaN UV photodetectors has prompted the development of similar devices based on wide bandgap $Al_xGa_{1-x}N$ semiconductors, in order to achieve shorter cut-off wavelengths. Of particular interest recently are "solar-blind" detectors which, by definition, are blind or insensitive to photons with wavelengths longer than ~280 nm.[25] This value of wavelength has been established from the fact that there are few photons from the Sun with a wavelength shorter than 285 nm which reach the surface of the Earth due to atmospheric absorption. A solar-blind detector at sea level would therefore not "see" the Sun, but only a closer object emitting UV photons. This was actually constituted the driving force behind the development of the entire compositional range of wide bandgap $Al_xGa_{1-x}N$ semiconductors.

The research work presented here is targeted towards solar blind UV p-i-n photodiodes for focal plane arrays. $Al_xGa_{1-x}N$ semiconductors with high Al concentrations are needed for this purpose in order to obtain a cut-off wavelength of λ~280nm, which raises technological difficulties in the growth and doping of the material, as well as the design and fabrication technology of the photodiode structure. The work reported here is focused on devices which were illuminated from the front (epilayer) side of the wafer.

VI.2. Experimental

The structure of the active region in solar blind p-i-n photodiodes must generally consist of $Al_xGa_{1-x}N$ layers with x>0.4, as shown in Figure 20. On the top of the active region, a very thin p-type GaN layer is generally included to allow for a better ohmic contact.

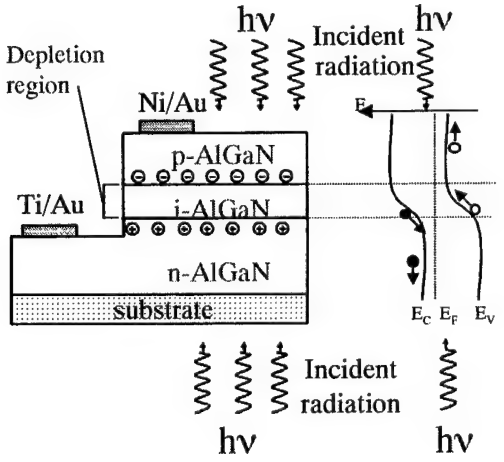

Figure 20. Device geometry and energy band diagram of AlGaN p-i-n photodiodes.

[25] P. Schreiber, T. Dang, T. Pickenpaugh, G. Smith, P. Gehred, and C. Litton, "Solar blind UV region and UV detector development objectives," *Part of the SPIE conference on Photodetectors: Materials and Devices IV, Proc. SPIE,* vol. 3629, edited by G. Brown, pp. 230-248 (SPIE Optical Engineering Press, Bellingham, 1999).

The AlGaN films and structures were grown in an Aixtron 200/4 HT, horizontal flow low-pressure metalorganic chemical vapor deposition (MOCVD) reactor. Hydrogen and nitrogen were employed as carrier gases. The elemental precursors included trimethylgallium, trimethylaluminum, and ammonia. Silane and biscyclopentadienylmagnesium were used as donor and acceptor dopant sources respectively. Double side polished basal plane sapphire substrates were employed. The details of the growth process have been reported earlier.[26,27] Prior to the active region growth, a ~2 μm thick n-type GaN template layer was grown. The thicknesses of the subsequent AlGaN n-, i- and p-type layers were 500~1000, 200 and 100~200 nm, respectively. Furthermore, a thin (50 Å) GaN:Mg cap layer was grown to reduce the metal p-contact resistance and facilitate carrier collection.

Upon removal from the growth chamber, the samples were annealed in an N_2 ambient for Mg activation. They were then cleaned using organic solvents and standard lithography followed to define the detector geometries. The detector mesas were realized through dry etching in a $SiCl_4$-based plasma, and they were deep enough to expose the n-type GaN. Electron-beam evaporation was used to deposit Ti/Au and Ni/Au metal contacts onto the n-type and p-type layers, respectively. No anti-reflective coating or passivation was used for these devices. The detectors were then mounted onto heat sinks for evaluation and the characteristics for a few of these devices are now highlighted.

VI.3. Photodetector characterization and discussion

The responsivity of the front illuminated AlGaN photodiodes was measured using a Xe lamp, monochromator, chopper, UV-grade focusing optics in a standard synchronous detection scheme. A calibrated, UV-enhanced Si detector was measured to determine the power density spectrum of the Xe lamp, which allowed to obtain the absolute current responsivity of the AlGaN detectors which is given by:

$$\textit{Equation 7.} \qquad R_\lambda = \frac{\lambda q}{hc}\eta_{ext} g$$

where λ is the wavelength of the incident light, q is the electron charge, h is Planck's constant, c is the speed of light, η_{ext} is the external quantum efficiency and g is the gain of the detector which has been assumed equal to unity.

The detectors were generally measured without bias, i.e. in the photovoltaic mode. The obtained spectral responsivity curves are shown in Figure 21. A wide range of $Al_xGa_{1-x}N$ p-i-n photodiodes were achieved with an Al concentration in the active region extending from 0 to 70 %. This corresponding peak responsivity wavelength could thus be controlled from 362 down to 225 nm. This the widest range of AlGaN based photodiodes which . These confirm that both

---

[26] P. Kung, A. Saxler, D. Walker, X. Zhang, R. Lavado, K.S. Kim, and M. Razeghi, "$Al_xGa_{1-x}N$ Based Materials and Heterostructures," in *III-V Nitrides*, ed. by F.A. Ponce, T.D. Moustakas, I. Akasaki and B.A. Monemar, Materials Research Society Symposium Proceedings, vol. 449, pp. 79-84, Pittsburgh: Materials Research Society, 1997.

[27] P. Kung, D. Walker, P. Sandvik, M. Hamilton, J. Diaz, I.-H. Lee, and M. Razeghi, "Schottky MSM photodetectors on GaN films grown on sapphire by lateral epitaxial overgrowth," in *Photodetectors: Materials and Devices IV,* ed. Gail J. Brown, SPIE Proceedings Series, vol. 3629, pp. 223-229, Bellingham, Wash.: SPIE-The International Society for Optical Engineering, 1999.

visible blind and solar blind photodetectors could be achieved using the same $Al_xGa_{1-x}N$ material system. The visible and solar blindness is generally estimated by calculating the rejection ratio which is the ratio of the values of responsivity between the peak response and that in the visible region on the right side of Figure 21. These photodetectors exhibited a visible and solar blindness of up to six orders of magnitude, which is the highest value ever reported for AlGaN p-i-n photodiodes.

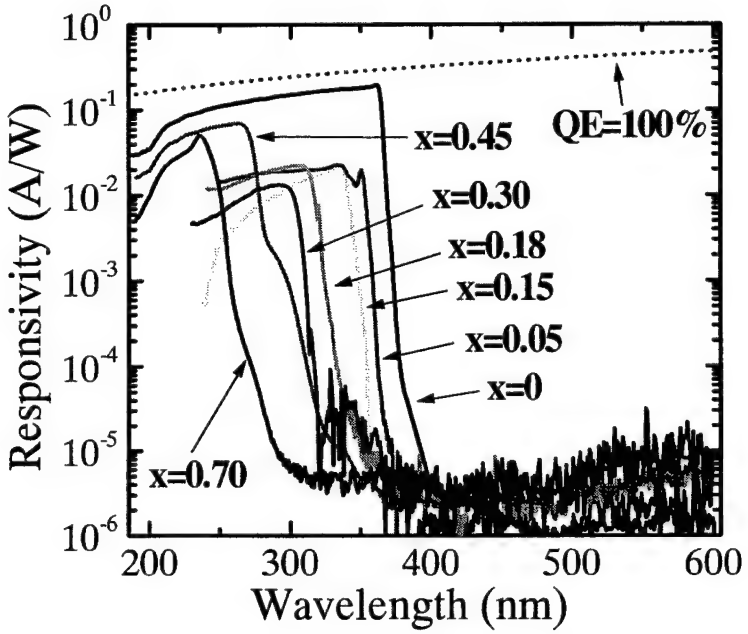

Figure 21. Responsivity curves for FI unbiased $Al_xGa_{1-x}N$ p-i-n photodiodes. The peak response covers much of the UV spectral region including the solar blind range. The theoretical limit for the peak responsivity of photodetectors with an external quantum efficiency of 100 % is also shown.

An example of a strictly $Al_xGa_{1-x}N$ p-i-n photodiode (i.e. x>0) exhibited a peak responsivity of 42 mA/W which could be measured at 232 nm, corresponding to an external quantum efficiency of 23 % without any applied bias. With a -5 V bias, the responsivity increased to 0.11 A/W, corresponding to an external quantum efficiency of 59 %, the highest external quantum efficiency reported to date for an $Al_xGa_{1-x}N$ based photodetector at such a short wavelength. This corresponded to an internal quantum efficiency higher than 90 %. The responsivity of these photodiodes was constant over three decades of incident optical powers.

VI.4. Summary

In summary, highly efficient $Al_xGa_{1-x}N$ based visible blind and solar blind p-i-n photodiodes have been demonstrated which cover the widest spectral range ever reported, form 225 to 362 nm. These photodetectors exhibited a very high visible and solar blindness, up to six orders of magnitude.

VII. ELECTROLUMINESCENCE OF DOUBLE HETEROSTRUCTURE LIGHT EMITTING DIODES WITH SI AND MG DOPED INGAN

We report in this section the growth, fabrication and electroluminescence measurements of double heterostructure GaN/InGaN light emitting diodes as a function of the doping type of the active layer.

The films were grown in a horizontal low-pressure metalorganic chemical vapor deposition reactor. Triethylgallium (TEGa), trimethylgallium (TMGa), trimethylindium (TMIn), biscyclopentadienylmagnesium (Cp_2Mg), dilute silane (SiH_4), and ammonia (NH_3) were used as precursors. All of the films were grown on (0001) Al_2O_3 substrates with a low temperature GaN buffer layer.

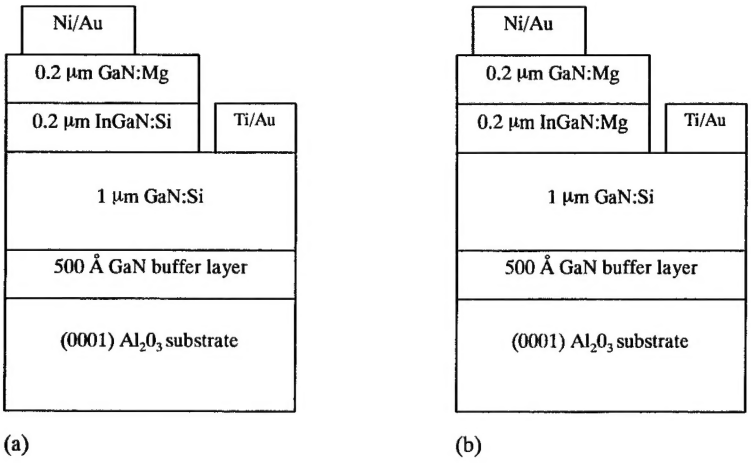

Figure 22. Schematic drawing of double heterostructures with (a) n-type and (b) p-type active layers.

Figure 22 shows schematic diagrams of the two double heterostructure devices which were grown and fabricated. After the buffer layer was deposited, a 1 μm thick silicon doped GaN layer with an electron concentration of 5×10^{18} was grown. This was followed by a 2000 Å InGaN active layer and a 2000 Å magnesium doped GaN layer. In the first structure the active layer was silicon doped, while in the second structure the active layer was magnesium doped. After dry etching down to the n-type layer, Ti/Au contacts were deposited. The p-type contacts were Ni/Au.

The I-V curves of the two diodes are shown in Figure 23. Both diodes exhibit low currents with reverse bias. The structure with the magnesium doped InGaN layer showed a lower turn on voltage than the structure with the silicon doped InGaN layer.

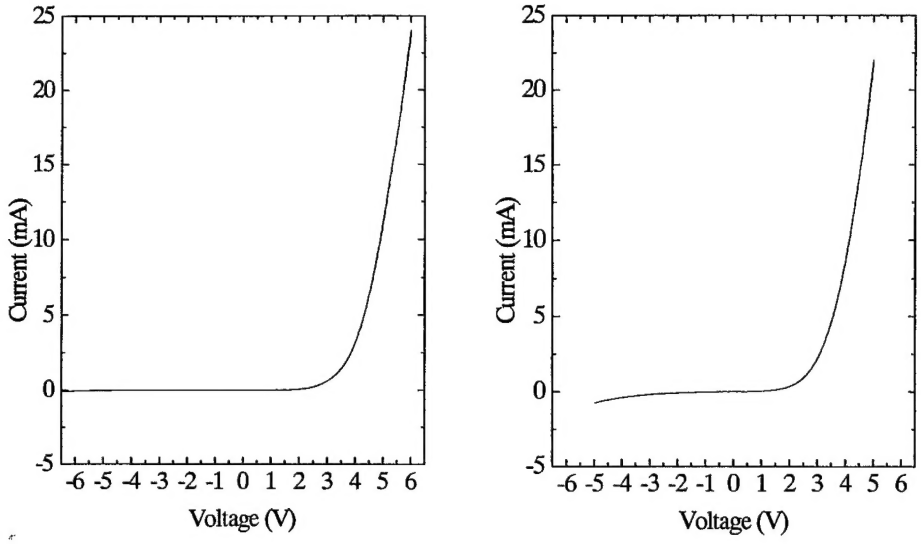

Figure 23. I-V curves of the double heterostructures with a (a) n-type and (b) p-type InGaN layer.

Figure 24 shows the electroluminescence curve of the double heterostructure with the silicon doped InGaN layer. A broad blue emission peak can be seen in the electroluminescence spectrum. The emission may be from magnesium related transitions in the GaN.

Figure 25 shows the electroluminescence of the structure with the magnesium doped InGaN layer. At low bias the red peak is dominant. As the bias is increased, the green peak begins to dominate. The green peak appears to be due to the magnesium related transition in the InGaN layer. The origin of the red peak is under further investigation. It is possible that the red peak is due to a transition metal (i.e. Cr) which has an absorption band in the green and a red emission band. This phenomenon is under investigation.

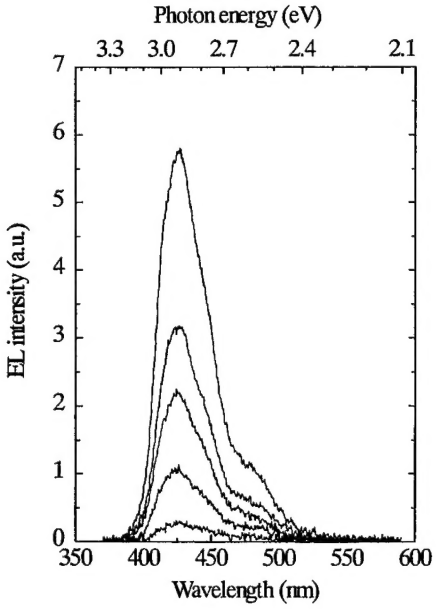

Figure 24. Voltage dependent electroluminescence spectrum of the structure with a silicon doped InGaN layer.

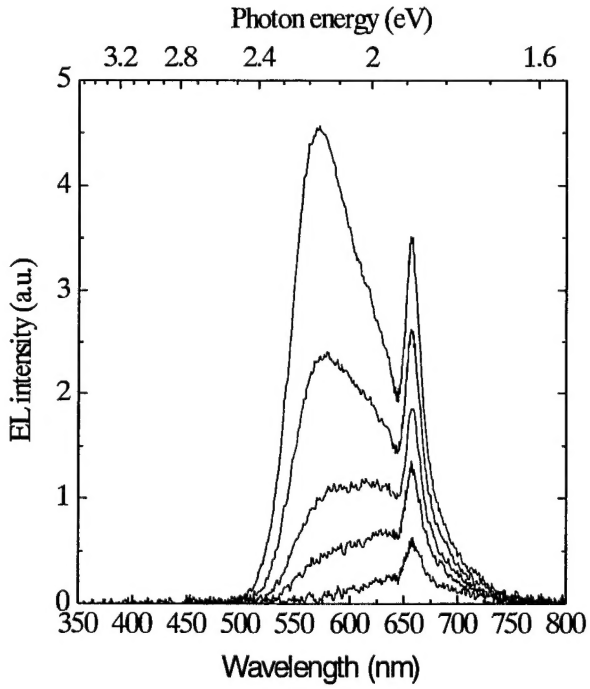

Figure 25. Voltage dependent electroluminescence spectrum of the structure with a magnesium doped InGaN layer.

VIII. SUMMARY

We have reported the MOCVD growth and characterization results for undoped, n-type and p-type doped wide bandgap GaN and $Al_xGa_{1-x}N$ semiconductors, for x ranging from 0 to 1, on sapphire substrates.

The optical and electrical properties of GaN films grown by MOCVD using two different organometallic precursors, TMGa and TEGa, have been compared.

We have reported the fabrication and characterization of n.i.d. GaN and GaN:Mg MSM photodetectors, with high speed and visible rejection.

GaN p-i-n photodiodes were grown by low-pressure MOCVD, which exhibited a UV-to-visible rejection ratio of 6 orders of magnitude.

The responsivity of these devices was analytically modeled and allowed the extraction of the minority carrier diffusion length for electrons in the p-type GaN material.

Highly efficient $Al_xGa_{1-x}N$ based visible blind and solar blind p-i-n photodiodes have been demonstrated which cover the widest spectral range ever reported, form 225 to 362 nm.

Finally, GaInN/GaN double heterostructures have been fabricated on sapphire substrates. By varying the doping of the GaInN active layer, blue (525 nm) and green (560 nm) light emitting diodes were demonstrated and characterized.